

# We are IntechOpen, the world's leading publisher of Open Access books Built by scientists, for scientists

6,900

Open access books available

186,000

International authors and editors

200M

Downloads

Our authors are among the

154

Countries delivered to

TOP 1%

most cited scientists

12.2%

Contributors from top 500 universities



WEB OF SCIENCE™

Selection of our books indexed in the Book Citation Index  
in Web of Science™ Core Collection (BKCI)

Interested in publishing with us?  
Contact [book.department@intechopen.com](mailto:book.department@intechopen.com)

Numbers displayed above are based on latest data collected.  
For more information visit [www.intechopen.com](http://www.intechopen.com)



# Development of Generic Radiating Model for Rectangular Capacitors: Magnetic Near Fields Analysis and Modeling

*Walid Labiedh, Bessem Zitouna, Mohamed Tlig  
and Jaleddine Ben Hadj Slama*

## Abstract

This chapter deals with modeling the radiation from rectangular film capacitors as a power electronics component. The rectangular film capacitors are sources of electromagnetic radiation, where its characterization is crucial for electronic circuits EMC. Our study presents the analyses and modeling of the magnetic near field radiated by the plastic and the polyester capacitors. An electromagnetic inverse method is combined with an optimization method based on genetic algorithms to create a radiating equivalent model. A very good agreement is observed between the magnetic near field cartography measured above the studied structure and calculated using the developed model parameters. Finally, a generic radiating model is proposed for various types of rectangular film capacitors. The generic model is validated using the measurements on a rectangular capacitor. The obtained equivalent model can calculate the magnetic field at any near field zone and far field around the capacitors. Circuit designers can use the field distribution to optimize the placement of the capacitors on the printed circuit board to reduce their coupling and potential interaction with other equipment in the vicinity of the system.

**Keywords:** Electromagnetic compatibility (EMC), Film capacitors, electromagnetic radiation, near field, inverse problems, generic model, analysis and modeling

## 1. Introduction

In power electronics, the switching frequencies are increasingly high to reduce these systems' weight, volume, and cost. This rise in frequency is accompanied by an increase in conducted and radiated electromagnetic disturbances. It also has significant effects on the behavior of these components at high frequencies. The characterization of the electromagnetic behavior of the various components of power electronics systems is an important step to control these systems' electromagnetic compatibility that should start from the design phase [1–4].

Many researchers have proposed radiating models for components or systems. In [2], concerning systems, a radiating model of a DC-DC converter was put forward and referenced as TEN 40–2412. The suggested model was composed of a network of four magnetic dipoles. The study in [3] proposed two radiating models

of a circuit based on a microcontroller. The first model was based on 53 magnetic dipoles, while the second one was based on 517 electric dipoles. In [4], a radiating model of the MOSFET was presented, constituted by a magnetic dipole. Two radiating models of toric self-inductance were suggested in [5]. The first developed model consisted of a large number of dipoles (676 dipoles). It was obtained by using a modeling approach based on the matrix inversion. The second model was composed of a network of 12 dipoles. Previously, researchers have already put forward a radiating model for an inductor [6, 7]. The proposed model by [6] consisted of a network of two simple magnetic dipoles. However, the one suggested by [7] was composed of a large number of magnetic and electric dipoles (520 dipoles). The measurements of the electromagnetic radiation were performed as described in [8].

On the other hand, several methods have been developed to model the radiated emissions of components and electrical systems. The study in [3] suggested two methods. The first one was based on magnetic dipoles, and the second one was based on electric dipoles. The two presented methods required both the field amplitude and phase. The study in [4] put forward an electromagnetic inverse method based on the Genetic Algorithms (GA). The method gave good results when the number of searched parameters is not very significant; otherwise, the method was inefficient considering calculation time and convergence. The same authors developed [2] a new approach based on image processing descriptor PZMI by processing only a scan window of the measured magnetic field cartography. Another approach was developed based on the matrix calculation [6, 7].

In this chapter, we are interested in the radiation of film capacitors. The film capacitors are widely used in the power electronics domain replacing electrolytic capacitors. They particularly permit the improvement of reliability and EMI suppression. Indeed, they are often used in new industrial applications, such as power converters for renewable energy and hybrid automotive systems. The film capacitors are mainly characterized by a high insulation resistance, large conduction currents, and good stability of its capacitance. These components are generally cumbersome, and their radiation certainly affects the overall radiation of the circuits. The electromagnetic field radiated by capacitors creates induced disturbances that may cause a dysfunction to the neighboring circuits. Therefore, the mastery of all the circuit's radiated fields is a requirement for the system's proper functionality. It will be worthwhile to dispose of the radiation model of capacitors.

The literature review of papers related to EMC analysis of discrete capacitors shows few studies dealing with conducted disturbances across these components and their coupling effects on other neighboring components. Particularly, in [9–12], the authors first studied the electromagnetic coupling between the components of an EMC filter. The filter was composed of two capacitors and two coils. Second, they proposed an automatic method to determine the optimal placement of components and the associated tracks' design. However, these studies treat the coupling only in EMC filter applications. They were not interested in the capacitor's radiation. In [12], methods for predicting the magnetic field distribution in the capacitors were presented. Although the existence of a magnetic field may seem anecdotal in capacitors whose functionality depends on the electric field, the magnetic field is precisely the cause of imperfections of the capacitors: the equivalent series inductance, the resonant frequencies, the associated losses, and the currents induced in metalized capacitors [13].

The present chapter aims to propose a radiation model for film capacitors, which has never been proposed before. In Section 2, the experimental techniques used to characterize the near field around the capacitors are presented. In Section 3, the magnetic near field above the capacitors is analyzed. The modeling method is explained in Section 4. In the following sections, the measured fields are used to

develop the radiating models of the studied capacitors. Finally, a generic model for all rectangular capacitors is presented.

## 2. Experimental techniques and characterization method

### 2.1 Excitation circuit

To allow characterization over a wide frequency band, the component under test (CUT) is excited by a current having a large frequency band similar to those found in power electronics. Therefore, It is proposed to install the component under test in a converter circuit supplied by a voltage equal to 30 V and has a duty cycle of 0.5 (**Figure 1**). The output current of the circuit is 0.5 A. The switching frequency is 50 kHz.

### 2.2 Measurements methods

In our study, we utilize only one component of the field radiated by the system under test. Indeed, the use of a single component in a large number of points is quite sufficient to identify the equivalent source by guaranteeing the uniqueness of the solution [14, 15]. Furthermore, the developed radiating model is capable of modeling the electric field as well as the magnetic field. Actually, based on [16–18], we can calculate from the magnetic field, the electric ones, and vice versa.

Since the method can be applied to any magnetic or electric field component, we have used the vertical component  $H_z$ . We may also utilize the other tangential components ( $H_x$  or  $H_y$ ). For measuring the magnetic near field, we place a magnetic probe above the device under test. It is a manually made probe consisting of a 1.6 mm radius circular loop connected to the central conductor on one side and the external shield of a coaxial cable on the other side. To capture the various components of the H-field, it is necessary to place the normal of the collinear loop to the desired component.

In our study, we use two methods for measuring the magnetic field around the component. The first method performs the near field measurements in the frequency domain, and the second one is performed in the time domain.

#### 2.2.1 Frequency measurements

The method of frequency measurements is based on a spectrum analyzer. In fact, to measure the magnetic field radiated of the under-test device, we use the near-field measurement bench presented in **Figure 2**.

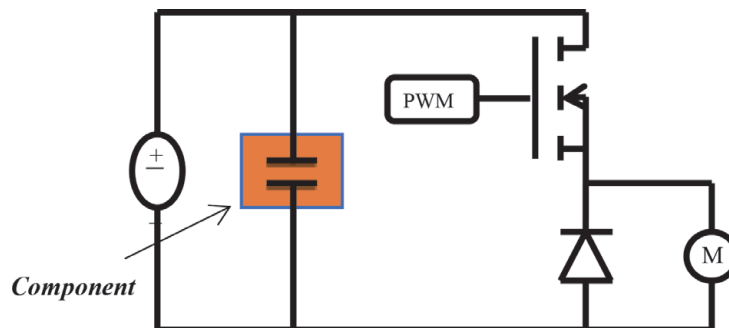


**Figure 1.**  
*Chopper circuit where component under test is characterized.*

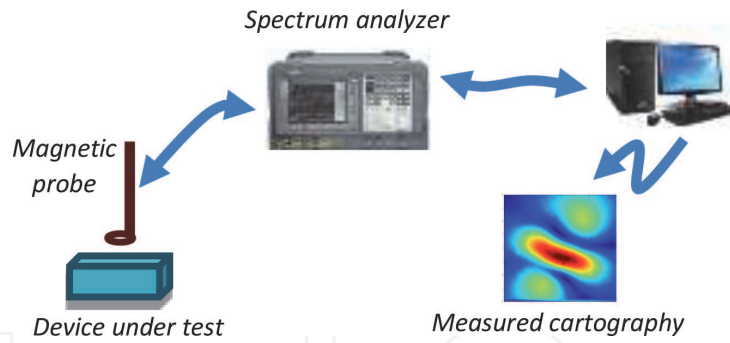


**Figure 2.**  
Frequency measurement bench.

### 2.2.2 Temporal measurements

The temporal measurements method is based on the utilization of an oscilloscope. This measurement method permits us to have a radiated magnetic field by the device under test at any moment. After measuring the temporal voltage across the probe, a Fast Fourier Transform (FFT) calculation is performed. **Figure 3** presents the adopted methodology.

According to Lenz-Faraday law, for a simple fixed circular conductor loop, having a very small radius  $R$  compared to the wavelength, diving in a magnetic field  $B(t)$  oriented along the  $z$ -axis, the potential difference induced in the loop by the magnetic field is given by the following equations:

In the time domain

$$V_m(t) = \oint \frac{\partial B}{\partial t} dS \quad (1)$$

In the frequency domain

$$V_m(f) = j \omega B S \quad (2)$$

where  $B = \mu_0 \times H$

$$\text{So } V_m(f) = j \omega \mu_0 H S \quad (3)$$

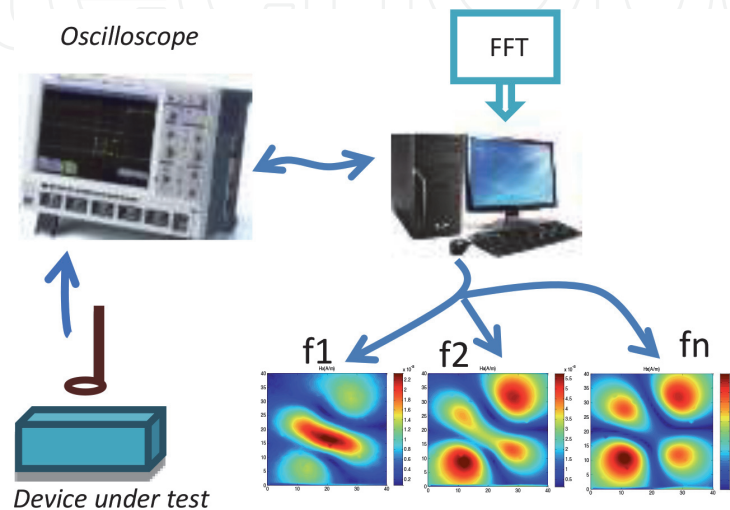


**Figure 3.**  
Methodology using temporal bench.

where  $\mu_0 = 4 \times \pi \times 10^{-7}$ , is the magnetic permeability  $S = \pi \times r^2$  is the surface of the probe,  $f$  is the radiation frequency, and  $\omega = 2\pi f$ .

The magnetic field is assumed to be constant over the entire area of the probe. This is especially true when the probe is very small compared to the capacitor's size. Therefore, the magnetic field measured at the center of the probe is calculated by the following equation:

$$H(f) = V_m(f) / 2 \times (2 \times \pi \times \mu_0 \times f \times 2 \times S) \quad (4)$$

where  $V_m(f)$  is the component at the frequency  $f$  of the FFT of the voltage measured at the terminals of the probe. Finally, we can extract the near-field cartographies for each radiating frequency.

### 2.3 Probe calibration

Before using a magnetic field probe, it is necessary to calibrate it. In [5, 6], the authors suggested a method to validate the accuracy of their magnetic field probes. They measured the radiated magnetic field around a simple circuit with a conductive wire above a ground plane. The values of the measured field are compared to those calculated theoretically. Thus, the comparison of the results enabled the validation of the used probes.

Similarly, in this work, to calibrate the magnetic probe, we have used a radiating circuit whose radiation is known theoretically. We compare the measured radiated magnetic field to that calculated by the numerical electromagnetic tool NEC [19] based on the moment's method. The radiating circuit is a rectangular loop of 5 cm length and 3 cm width excited by a sinusoidal voltage of 10 V amplitude at a frequency of 5 MHz (Figure 4).

The simulations and measurements are made at the points located in a horizontal plane at 3 mm above the radiating loop and having dimensions of  $5 \times 3 \text{ cm}^2$ . The calculation step is 2.5 mm along the X-axis and 1.5 mm along the Y-axis (441 measurement points).

Figures 5–7 gives the magnetic field components  $H_z$ ,  $H_x$ , and  $H_y$  along the X- and Y-axis, respectively. It shows a good agreement between the measured and calculated curves of the  $H_z$  component. In order to have a good signal-to-noise ratio when measuring  $H_x$  and  $H_y$  components, we chose measurement lines located at the edge of the emitting loop. Consequently, in some probe measurements, we notice a difference between measurements and simulations due to the edge effects and the coupling effects between the probe and the radiating loop. These phenomena are not significant on the  $H_z$  component and therefore do not affect the construction of the model.

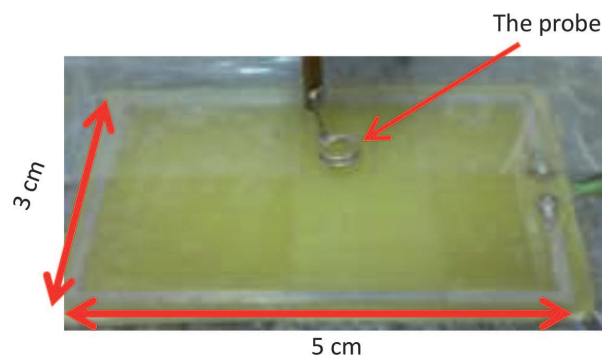


**Figure 4.**  
*Loop used for probe calibration.*

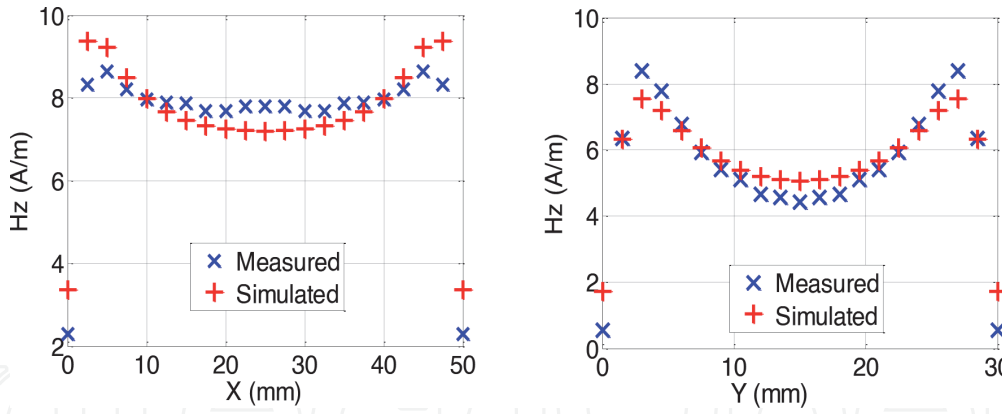


**Figure 5.**  
Hz following X- and Y-axes respectively for  $Y = 4.5$  mm and  $X = 25$  mm.

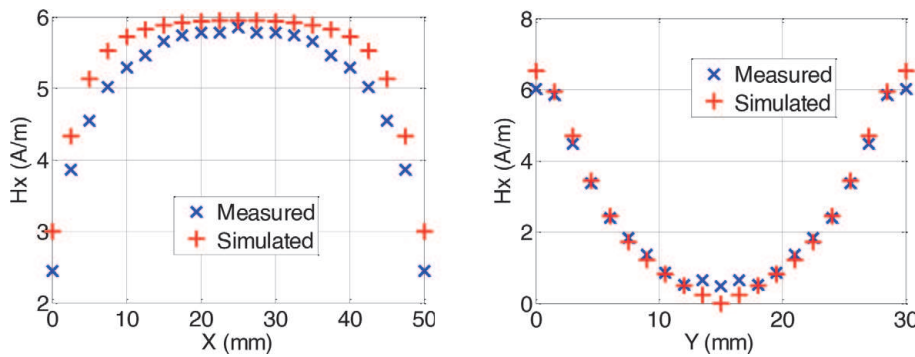


**Figure 6.**  
 $H_x$  following X- and Y-axes respectively for  $Y = 1.5$  mm and  $X = 25$  mm.

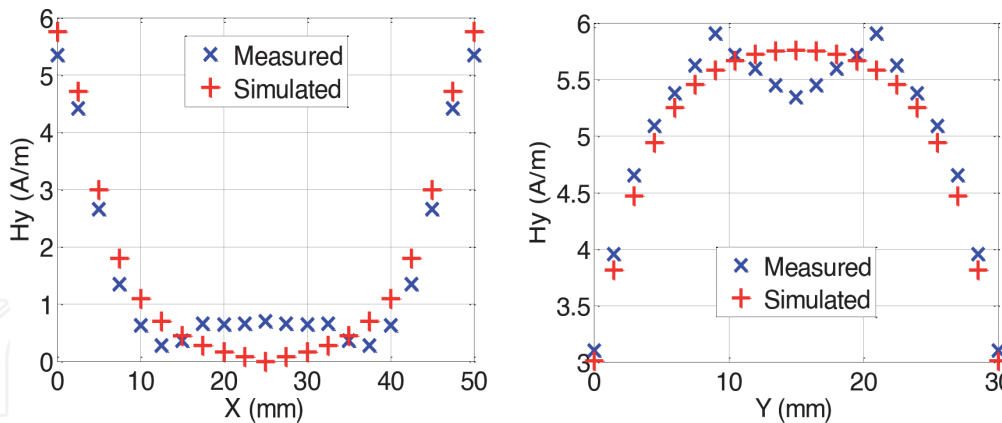


**Figure 7.**  
 $H_y$  following X- and Y-axes respectively for  $Y = 1.5$  mm and  $X = 25$  mm.

In order to examine the electric field rejection capability of our magnetic probe, we have placed it over a transmitting electric antenna where the amplitude of the electric field is important. The observed voltage across the probe is so low that we cannot dissociate it from the noise. Hence we deduce that our shielded probe rejects very well the electric field and measures the magnetic field with great accuracy.

### 3. Measurements and analysis of polypropylene capacitor radiation

Measurements are performed in the time domain using a high-bandwidth oscilloscope. We have measured the vertical component  $H_z$  of the magnetic near-field

radiated above a plastic polypropylene capacitor of a 2.2  $\mu\text{F}$  capacitance and a maximum voltage of 100 V (the capacitor size is 15 mm  $\times$  6 mm  $\times$  26.5 mm). To avoid the interferences caused by the capacitor legs, we have folded the legs of the latter. The probe is located at a distance of 2 mm above the capacitor in a plane whose dimensions are 4 cm  $\times$  2 cm. The displacements are done with a measuring step of 2 mm on the X-axis and 1 mm on the Y-axis. Thus, we have 400 measurement points. **Figure 8** shows the measurement plane and the component under test. It gives a particular point (3, 5) position in the measurement plane.

**Figure 9** shows the temporal voltage measured at the terminals of the magnetic probe once it is situated at the point (3, 5): the third position along the X-axis and the fifth position along the Y-axis. When analyzing the measured magnetic field signal, the existence of switching transients is noticed during turning on and off the power component utilized in the chopper.

We present in **Figure 10** the spectrum of radiated magnetic field Hz above the capacitor in the point (3,5). **Figure 10** shows the spectrum analysis of the whole temporal signal with both switching phases (closing and opening of the MOSFET in the excitation circuit where our studied component is characterized). That measured above the capacitor at the point of the coordinates (3,5) presented in **Figure 9**. By analyzing the measured temporal signal spectrum, four principal harmonics are observed, which have the following frequencies: 3 MHz, 11 MHz, 20 MHz, and 40 MHz. The resonances that appear above the capacitor are principally due to the

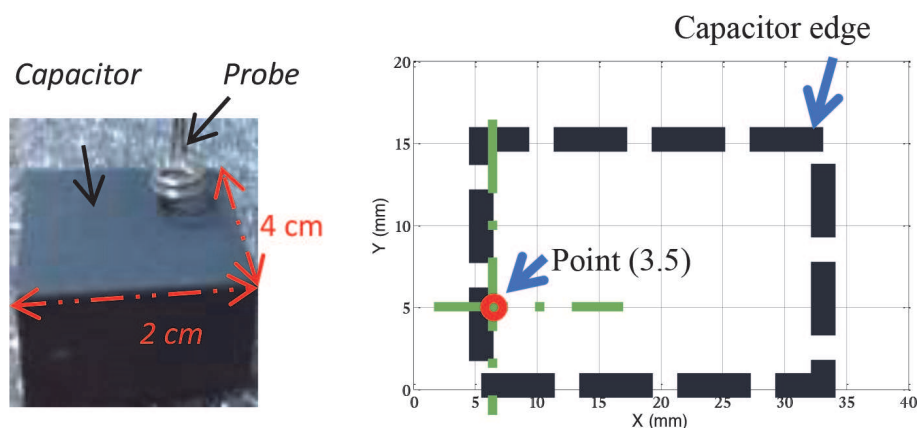


**Figure 8.**  
*Measurement plane over component under test.*

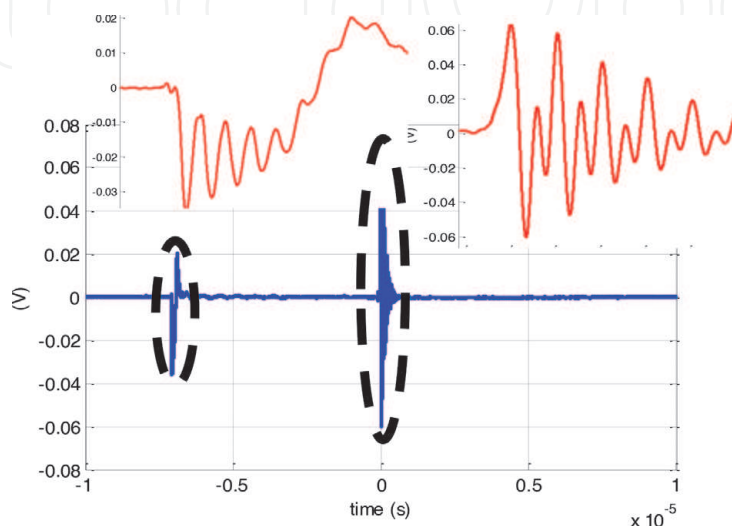


**Figure 9.**  
*Measured voltage at the terminals of the probe above capacitor under test.*

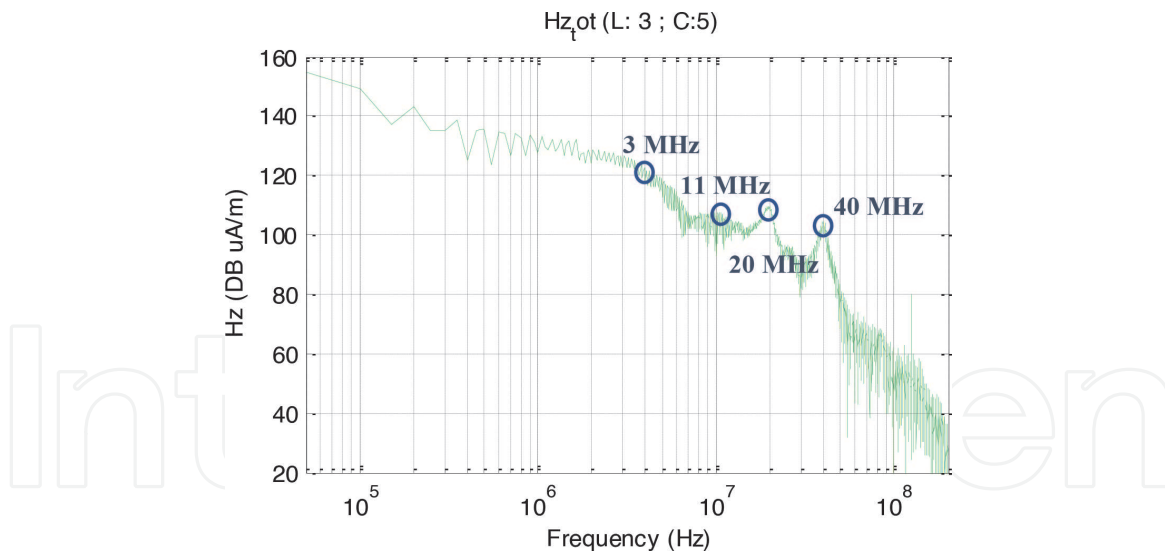


**Figure 10.** Spectrum of radiated magnetic field Hz at the terminals of the probe above the studied capacitor at point (3.5).

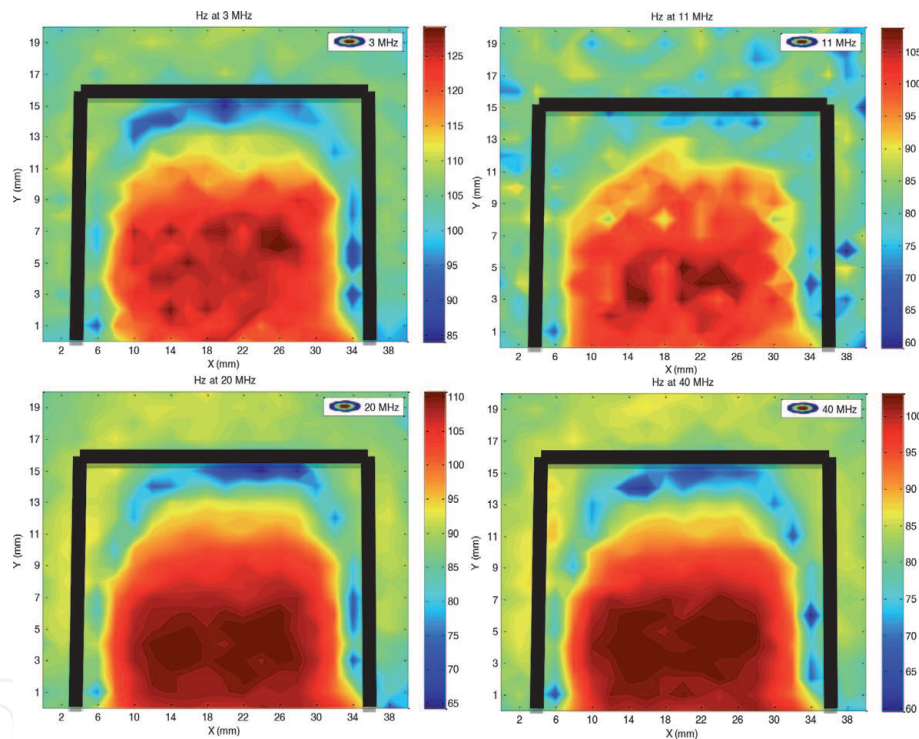


**Figure 11.** Cartographies of the near field for 3 MHz, 11 MHz, 20 MHz, and 40 MHz frequencies.

operating current flowing into the chopper circuit. **Figure 11** presents the cartographies of the field above the capacitor at these different frequencies.

According to the previous cartographies, the distribution of the radiated magnetic field above the capacitor is over the entire component surface, as illustrated in **Figure 12**.

#### 4. Modeling methodology

To develop a radiating model that enables producing a near field equal to that is radiated by the system under test, we use the flow diagram given in **Figure 13**. The modeling methodology is based on a hybrid approach consisting of the coupling between the electromagnetic inverse method and the Method of Moments (MoM) [20].

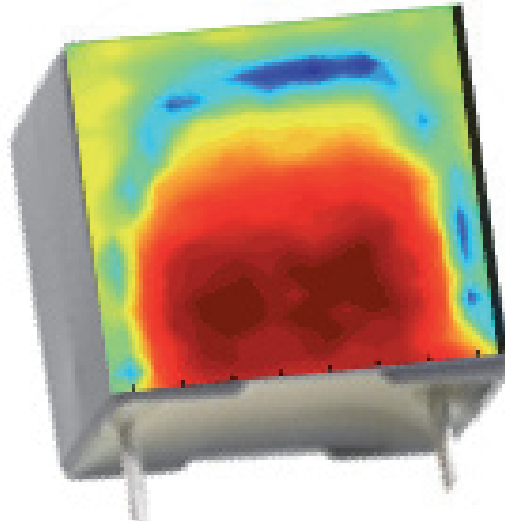


**Figure 12.**  
 Distribution of magnetic field above capacitor for  $f = 20$  MHz.

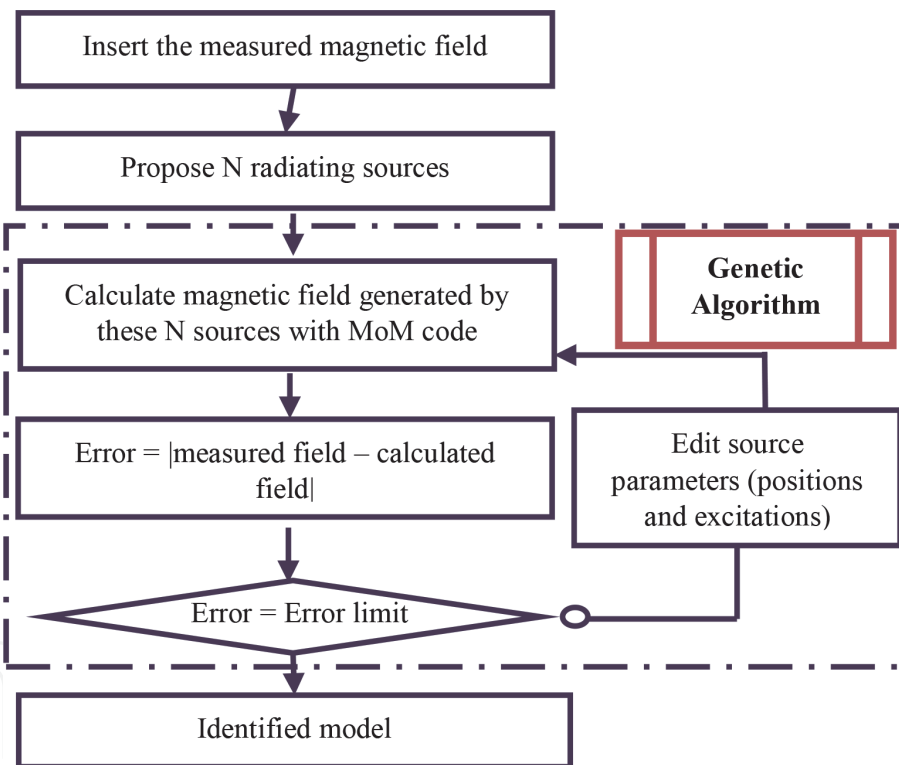


**Figure 13.**  
 Flow chart of the modeling approach.

This approach starts by introducing the electromagnetic near field measured around the device under test and then defines the optimization parameters by the Genetic Algorithm (GA) that has been presented in [21, 22]. After, the search is launched to find the parameters of the equivalent radiating structure by comparing the measured cartography to the one calculated numerically by the MoM and using the obtained parameters.

The magnetic field generated by the  $N$  sources is calculated using NEC2D software core, which is based on the MoM.

As the capacitor cartographies gather at the radiation of a rectangular loop, the search for models has been launched to find a rectangular current loop using the method based on the coupling between the inverse method and the MoM. Each

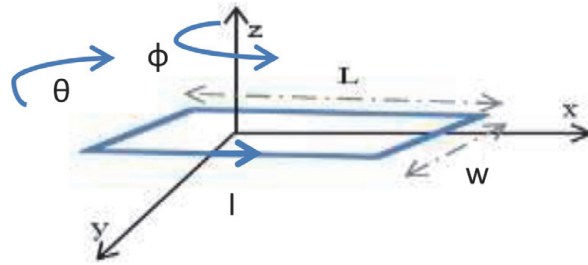


**Figure 14.**  
*Rectangular current loop parameters.*

rectangular loop is characterized by the coordinates of its center ( $X_0, Y_0, Z_0$ ), its width ( $w$ ), its length ( $L$ ), its orientations ( $\varphi, \theta$ ), the radius ( $r$ ) of the loop wire, and the current flowing through it (**Figure 14**).

## 5. Model for the polypropylene capacitor

### 5.1 Model research

After presenting the magnetic field cartography radiated by the capacitor in Section 3, we apply our approach to find a model that gives the same radiation as measured over the capacitor. To do this, we used the cartography of the vertical component  $H_z$  of the magnetic field at a frequency of 20 MHz. We chose the cartography of 20 MHz because it was the clearest one. **Figure 15** shows the position of the identified loop on the capacitor cartography. The modeling results for the obtained model are shown in **Table 1**.

**Figure 16** presents the measured and estimated cartographies of the magnetic field vertical component  $H_z$ . A reasonable agreement between the two cartographies is observed.

### 5.2 Model validation

Further validation of the model is performed on other faces of the capacitor or other components as proposed in [4, 23]. Hence, we measured the magnetic field cartography in the literal face and compared it to the one that has been calculated using the obtained model.

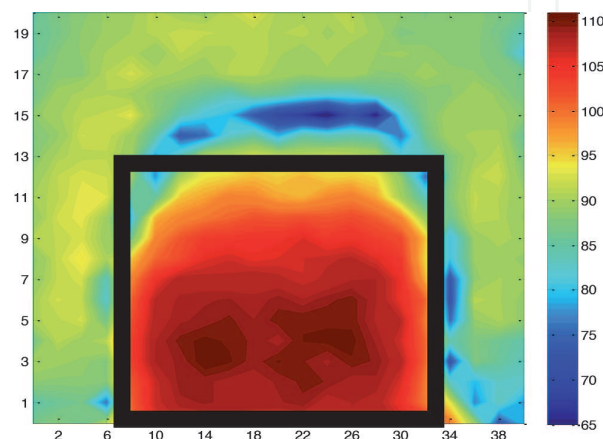


**Figure 15.**  
*Obtained loop position.*

Center coordinates ( $X_0, Y_0, Z_0$ ) (mm)	3.6; 19; -2.9	
Loop dimensions	Width (mm)	12
	Length (mm)	23
Orientations	$\varphi$ (rd)	0
	$\theta$ (rd)	0
Conductor radius R (mm)	1	
Voltage excitation (V)	0.035	

**Table 1.**  
 Parameters of the equivalent model of the polypropylene capacitor.

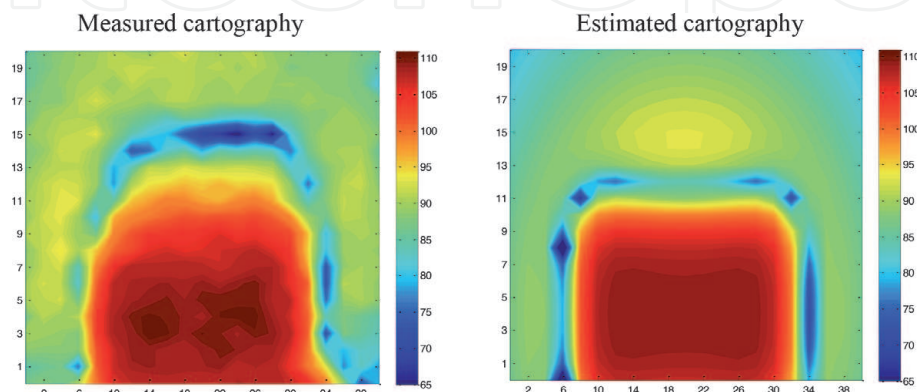


**Figure 16.**  
 Measured and estimated cartographies.

Accordingly, the capacitor is placed vertically, and measurements of the cartography are carried out on the other side of the capacitor. **Figure 17** depicts the layout of the measurements.

The validation of the model is made at 20 MHz and a measurement height of 3 mm. **Figure 18** shows the measured and calculated magnetic field cartography above the vertically placed capacitor.

According to the previous results, the magnetic field is reconstructed by the model shows good resembling with the measured one. These results confirm the existence of an equivalent rectangular current loop in the capacitor. To explain the obtained results, we present in **Figure 19** the internal structure of the capacitor. Film capacitors are made out of two pieces of plastic film covered with metallic electrodes wound into a cylindrical-shaped winding, with terminals attached, and then encapsulated.

The analysis of the internal structure of the film capacitor confirms the obtained equivalent model. Indeed, the surface of the capacitor appears as a rectangular loop.

The internal coupling phenomenon certainly causes this current distribution at the capacitor contour in the component. This current distribution in the capacitor film is consistent with that introduced in [12, 13].

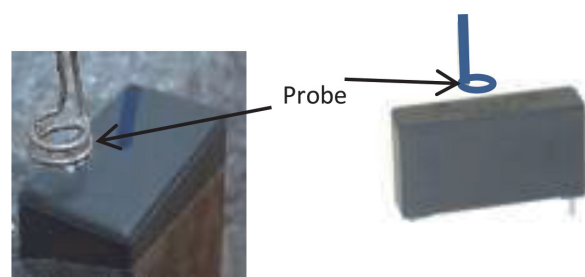


**Figure 17.**  
 Measurement of the magnetic field over a vertically placed capacitor.

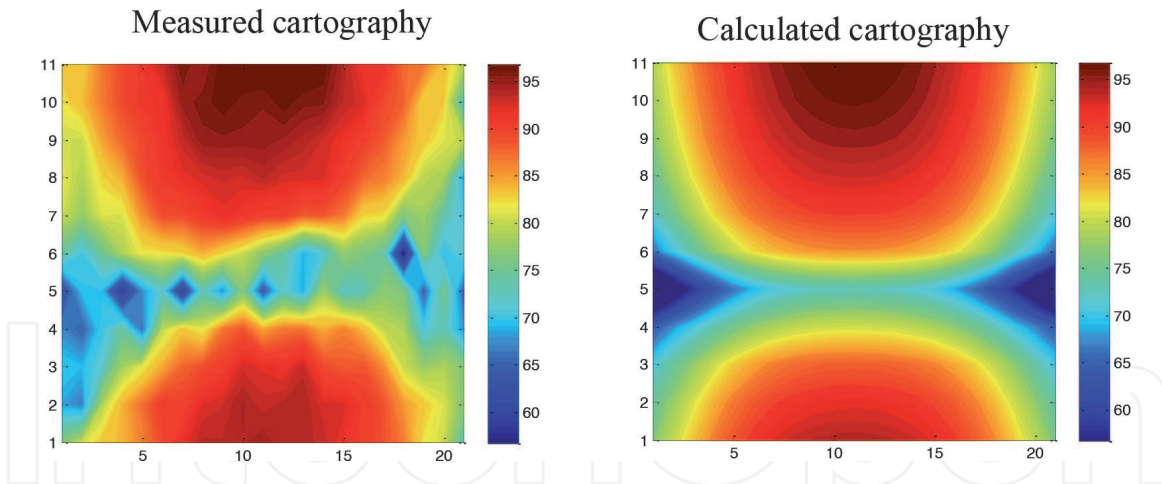


**Figure 18.**  
Cartographies of the measured and calculated field above vertically placed capacitor.

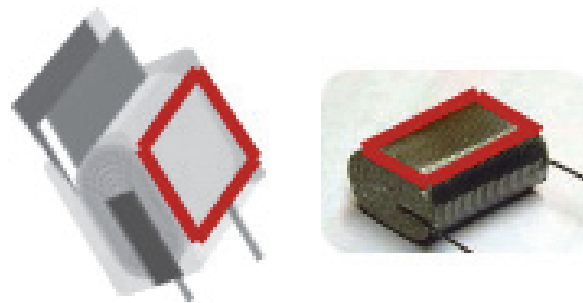


**Figure 19.**  
Film capacitor's internal structure.

## 6. Model for the metalized polyester capacitor

### 6.1 Measurement of magnetic near-field radiated by polyester capacitors

Based on the frequency measurement method, we measured the vertical component  $H_z$  of the magnetic field radiated above a metalized polyester capacitor of a  $1 \mu\text{F}$  capacitance and having a maximum voltage of 100 V (the capacitor size 14 mm x 7 mm x 18 mm). In order to have only the magnetic field radiated by the capacitor, the capacitor legs are bent. The probe was located at a 3 mm distance from the capacitor. The magnetic field measurements were performed in a plane whose dimensions were 30 mm x 20 mm with a measuring step of 1.5 mm on the X-axis and 1 mm on the Y-axis. **Figure 20** shows the measurement plane and the component under test.

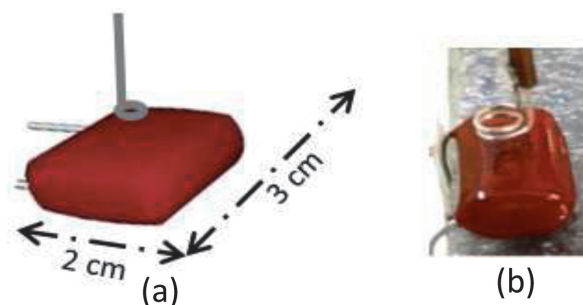


**Figure 20.**  
(a) Measurement plan; (b) device under test.

After making Fast Fourier transformation (FFT) of the measured signals above the capacitor, we notice that the frequency of 26 MHz has maximum amplitude. We present in the following **Figure 21** the cartographies of the Hz and Hy components measured at the frequency of 26 MHz.

## 6.2 Radiated-field modeling

As for the polypropylene capacitor, the radiation of the polyester capacitor looks like that of a rectangular loop. The same method exposed previously is used to the cartography of the measured magnetic field Hz at the frequency of 26 MHz. The modeling result is a rectangular current loop whose parameters are given in **Table 2**. **Figure 22** exposes the cartographies of the magnetic field Hz measured and estimated by the obtained model above the capacitor. A good agreement between the two cartographies is observed.

## 6.3 Model validation

To validate the obtained model better, we examined the cartographies of the other components of the magnetic field above the capacitor. We specifically compared the measured component, Hy of the magnetic field, calculated using the obtained model (**Figure 23**).

The previous results show that the magnetic field reconstructed by the model resembles, to a great extent, the measured magnetic field.

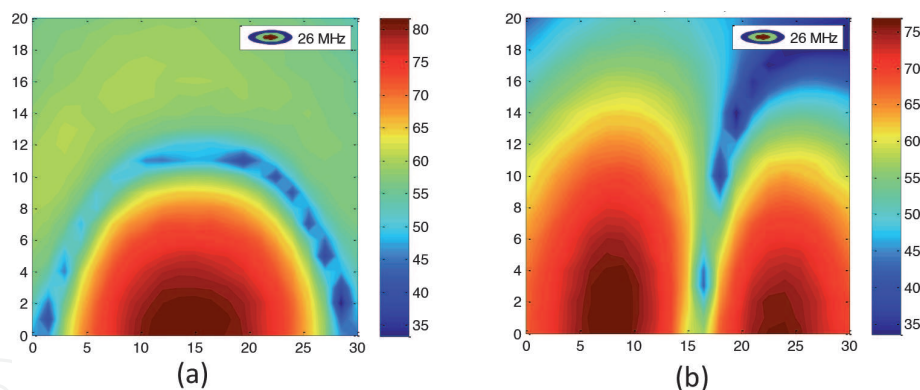


**Figure 21.** Cartographies of the field above the capacitor: (a) Hz and (b) Hy.

Center coordinates ( $X_0, Y_0, Z_0$ ) (mm)		1; 15; -3.3
Loop dimensions	Width (mm)	12
	Length (mm)	16
Orientations	$\varphi$ (rd)	0
	$\theta$ (rd)	-0.2
Conductor radius R (mm)		1
Voltage excitation (V)		0.0017

**Table 2.** Parameters of the equivalent model of the metallized polyester capacitor.

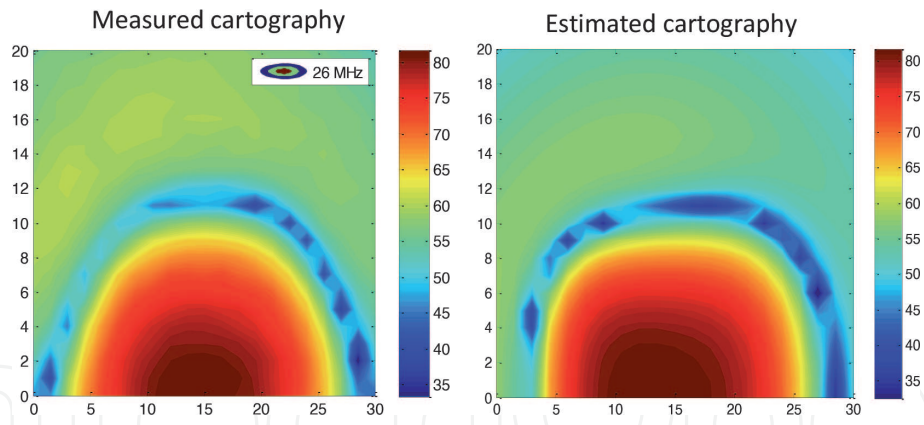


**Figure 22.**  
Measured and estimated cartographies of polyester capacitor.

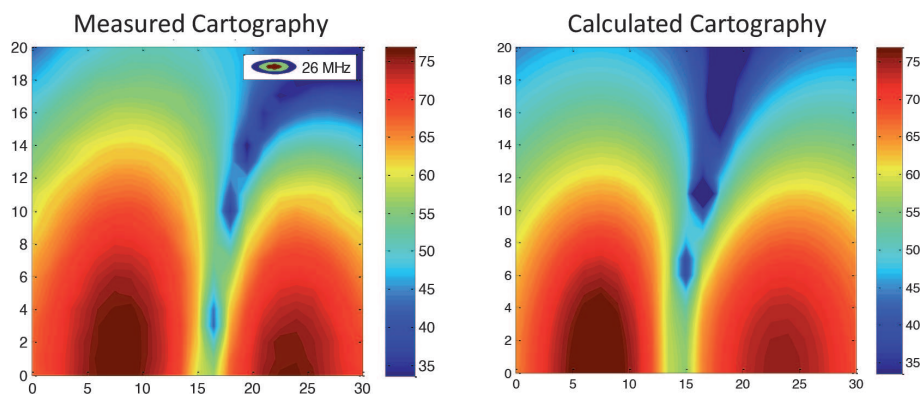


**Figure 23.**  
Cartographies of measured and estimated  $H_y$  component of the magnetic field above the capacitor.

## 7. Capacitor generic model

The examination of the results obtained previously allows us to conclude that the equivalent radiating model for the different types of rectangular film capacitors is a rectangular loop whose parameters depend on the geometry of the capacitor as illustrated in **Figure 24** and explained in **Table 3**.

We suggest in **Table 3** formulas in order to determine by using capacitor dimensions the size of the source rectangular loop of the generic model.

To validate the proposed generic model, we applied it to another rectangular capacitor. Therefore, we measured the magnetic field above a third rectangular

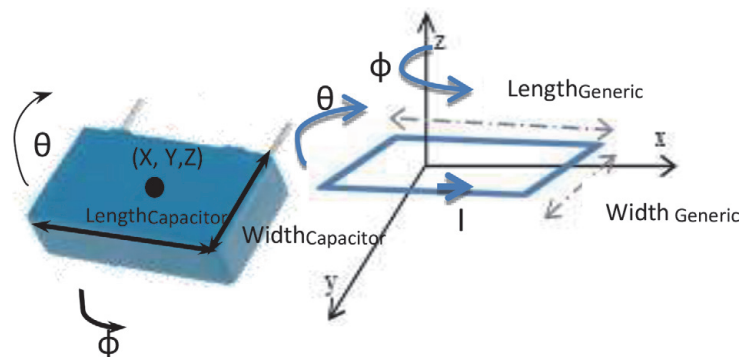


**Figure 24.**  
Capacitor parameters and the analogy with the equivalent loop.

The center coordinates	The Gravity center of the capacitor
Loop dimensions	Width <sub>Generic</sub> $\cong 0.8 \times$ Width <sub>capacitor</sub> Length <sub>Generic</sub> $\cong 0.86 \times$ Length <sub>capacitor</sub>
Orientations	$\varphi = 0$ $\theta$ depends on the position of the capacitor under test relative to the x-axis $\cong 0$ .
Voltage excitation	Dependence on the field amplitude

**Table 3.**  
 Size of the source rectangular loop of the generic model.

capacitor having 2.2  $\mu$ F capacitance and a maximum voltage of 250 V (the capacitor size is 25 mm x 14 mm x 41.5 mm).

We performed measurements of the near field cartography above the studied capacitor, and then we applied the method based on the coupling of the electromagnetic inverse method with the MoM to find the equivalent model that will be compared to the one obtained by the generic model formulas.

According to **Table 4**, we notice that the calculated parameters by the formulas of the generic model are very close to those obtained by the inverse electromagnetic method.

We observe from the previous table that the searching model using the generic model is seven times faster than when being used without the generic model. Indeed, in the generic model, we search only one parameter (the excitation voltage), while the others parameters are calculated using the formulas given in **Table 3**.

**Figure 25** shows  $H_y$  and  $H_z$ 's components of the magnetic near-field measured and estimated by the two obtained models above the capacitor under test at a frequency of 27 MHz.

According to the previous results, the magnetic field reconstructed using the proposed generic model shows an agreement with the measured magnetic field. In fact, in our modeling approach, we are interested in the high amplitudes of the magnetic field (red parts in the cartographies) because they have the most important magnetic field radiated by the component under test. We notice a good agreement between the measured and calculated fields by the generic model is observed.

**Figure 26** presents a comparison between the two models for cuts of  $H_z$  and  $H_y$  components along the x-axis. It shows a reasonable agreement between the measured magnetic field and the obtained one with the two models.

	Without generic model	Generic model
The center coordinates ( $X_0, Y_0, Z_0$ ) (mm)	2; 26; -7.3	2.3, 25, -7
Loop dimensions	Width (mm)	21
	Length (mm)	37
Orientations	$\varphi$ (rd)	0
	$\theta$ (rd)	0
Conductor radius R (mm)	1	1
Voltage excitation (V)	0.0007	0.00055
Modeling time (min)	62	8

**Table 4.**  
 Parameters of rectangular loop obtained by two methods.

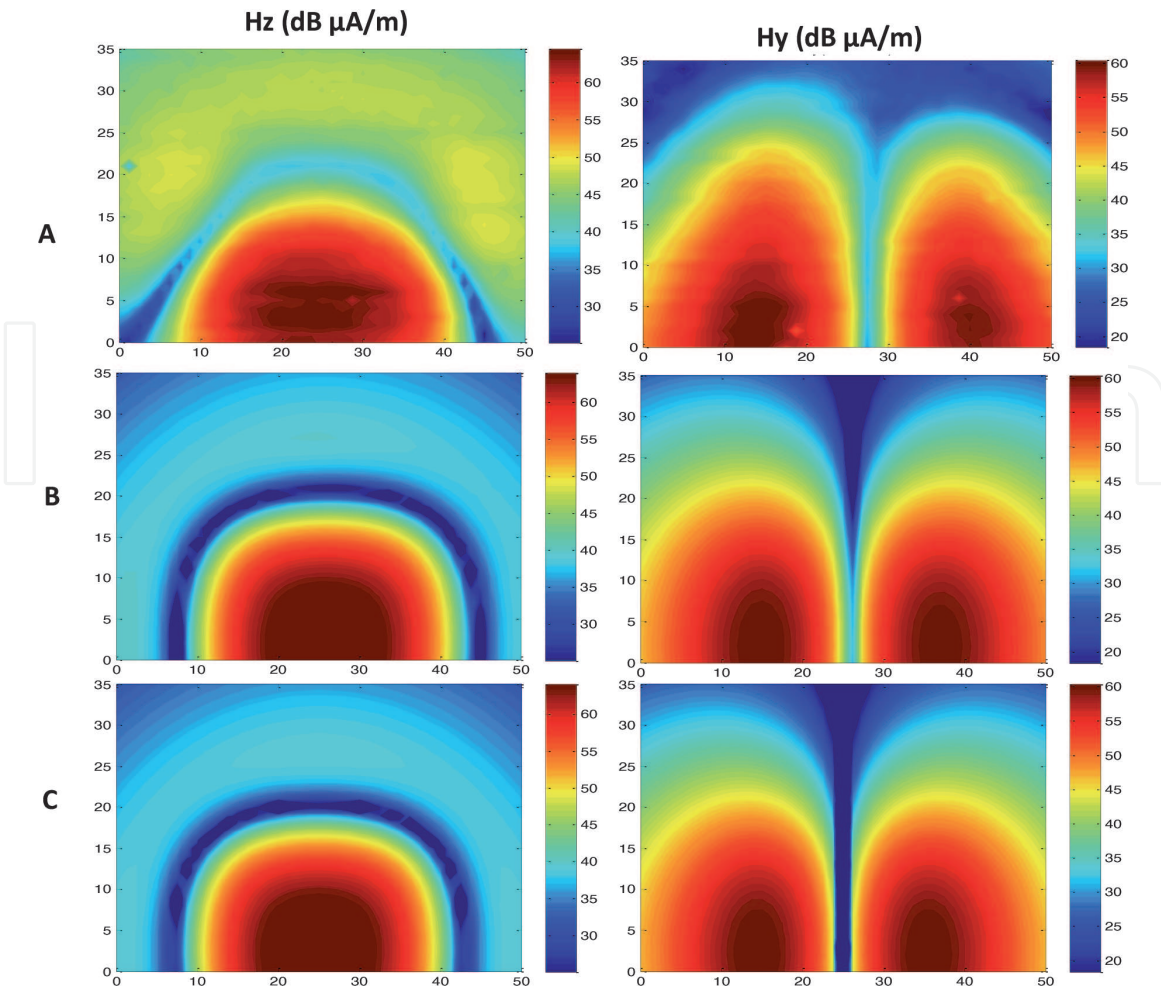


**Figure 25.** Cartographies of magnetic field: (A) measured and (B) estimated using the inverse method and (C) using generic model (at 27 MHz).

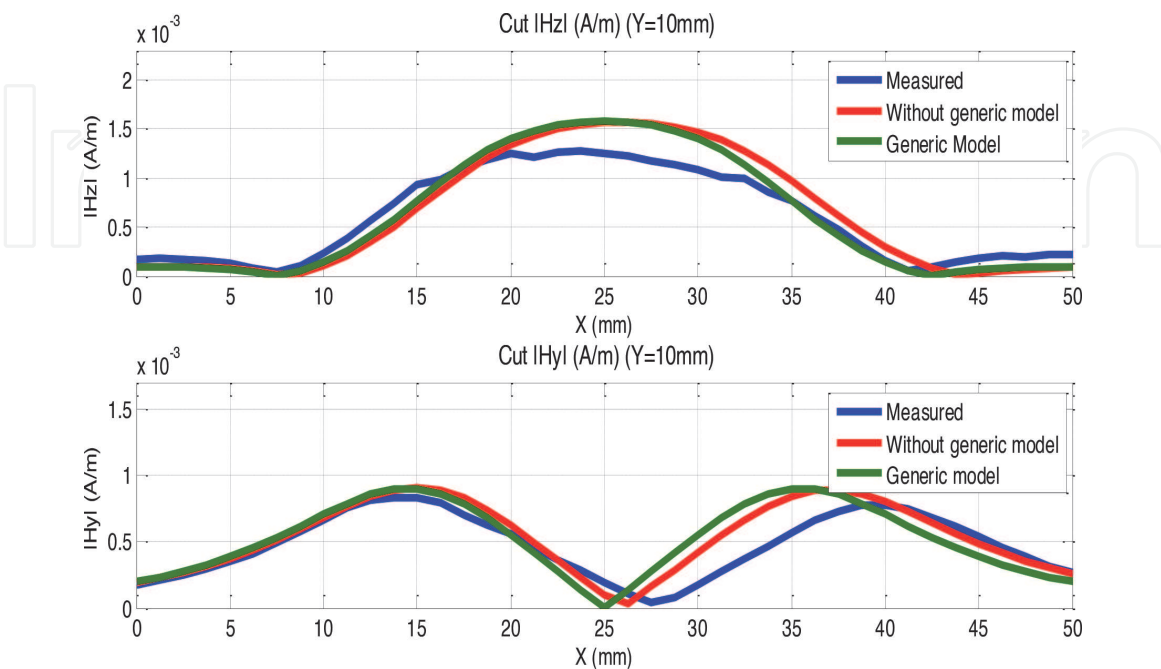


**Figure 26.** Comparison of the two models for cuts of  $H_z$  and  $H_y$  components along the  $x$ -axis.

The examination of all the obtained results enables us to conclude that the suggested generic model is a slight model that permits, in a very short time, the calculation of the radiation of the different types of rectangular capacitors.

## 8. Conclusion

Film capacitors are among the larger components on power electronics boards. Therefore, they cause considerable radiation above all the circuits. In this paper, we have presented the characterization measurements of the magnetic field radiated by different film capacitors used in power electronics. We have then utilized the inverse electromagnetic method based on coupling between the Genetic algorithms and the MoM to find models of equivalent radiating sources of these capacitors. A generic radiating model for different rectangular film capacitors has been finally put forward and validated using measurements on another capacitor.

This equivalent model is special; hence, its radiation is much more complicated than the one usually used by the electromagnetic inverse problem (elementary magnetic and electric dipoles).

The proposed radiating model reduces the number of parameters to be determined by the GA method and consequently reduces the convergence time of the inverse method. Circuit designers can use it to optimize the placement of capacitors on the printed circuit board to reduce their coupling with other equipment located in the vicinity of this system.

### Author details

Walid Labiedh, Bessem Zitouna\*, Mohamed Tlig and Jaleddine Ben Hadj Slama  
LATIS, Laboratory of Advanced Technology and Intelligent Systems, ENISo,  
National Engineering School of Sousse, University of Sousse, Tunisia

\*Address all correspondence to: [bessem.zitouna@yahoo.fr](mailto:bessem.zitouna@yahoo.fr)

### IntechOpen

© 2021 The Author(s). Licensee IntechOpen. This chapter is distributed under the terms of the Creative Commons Attribution License (<http://creativecommons.org/licenses/by/3.0>), which permits unrestricted use, distribution, and reproduction in any medium, provided the original work is properly cited. 

## References

- [1] Jaleddine BEN HADJ SLAMA and Walid LABIEDH, "Library of EMC Models for Passive Components and Printed Circuit Board," Electrotechnical Conference (MELECON), 16th IEEE Mediterranean, pp. 325-330, 25-28 March 2012.
- [2] Saidi, S.; Ben Hadj Slama, J., "A Near-Field Technique Based on PZMI, GA, and ANN: Application to Power Electronics Systems," IEEE Transactions on Electromagnetic Compatibility, VOL. 56, no. 4, pp. 784-791, Aug. 2014.
- [3] Y. Vives-Gilabert, C. Arcambal, A. Louis, F. De Daran, P. Eudeline, B. Mazari, "Modeling Magnetic Radiations of Electronic Circuits Using Near-Field Scanning Method," IEEE Transactions on Electromagnetic Compatibility, VOL. 49, no.2, pp.391-400, May 2007.
- [4] Sofiene Saidi and Jaleddine Ben Hadj Slama, "Analysis and modeling of power MOSFET radiation," Progress In Electromagnetics Research M, VOL. 31, pp 247-262, 2013.
- [5] Yolanda Vives-Gilabert, Christian Arcambal, Anne Louis, Philippe Eudeline, and Belahcene Mazari, "Modeling Magnetic Emissions Combining Image Processing and an Optimization Algorithm" IEEE Transactions on Electromagnetic Compatibility, VOL. 51, NO. 4, pp 909-918, NOVEMBER 2009.
- [6] Levy, P.-E.; Gautier, C.; Costa, F.; Revol, B.; Labarre, C., "Accurate Modeling of Radiated Electromagnetic Field by a Coil With a Toroidal Ferromagnetic Core," IEEE Transactions on Electromagnetic Compatibility, VOL. 55, no. 5, pp. 825-833, Oct. 2013.
- [7] Shall, H.; Riah, Z.; Kadi, M., "A 3-D Near-Field Modeling Approach for Electromagnetic Interference Prediction," IEEE Transactions on Electromagnetic Compatibility, VOL. 56, no. 1, pp.102-112, Feb. 2014.
- [8] Baudry, D.; Arcambal, C.; Louis, A.; Mazari, B.; Eudeline, P., "Applications of the Near-Field Techniques in EMC Investigations," IEEE Transactions on Electromagnetic Compatibility, VOL. 49, no. 3, pp. 485-493, Aug. 2007.
- [9] De-Oliveira, T.; Schanen, J.-L.; Guichon, J.-M.; Gerbaud, L., "Optimal Stray Magnetic Couplings for EMC Filters," IEEE Transactions on Industry Applications, VOL. 49, no. 4, pp. 1619-1627, July-Aug. 2013.
- [10] De Oliveira, T.; Guichon, J.-M.; Schanen, J.-L.; Gerbaud, L., "PEEC-models for EMC filter layout optimization," 2010 6th International Conference on Integrated Power Electronics Systems (CIPS), VOL., no, pp. 1-6, 16-18 March 2010.
- [11] Henglin Chen; Zhaoming Qian, "Modeling and Characterization of Parasitic Inductive Coupling Effects on Differential-Mode EMI Performance of a Boost Converter," IEEE Transactions on Electromagnetic Compatibility, VOL. 53, no. 4, pp. 1072-1080, Nov. 2011.
- [12] E. L. Nativel, T. Talbert, T. Martire, C. Joubert, N. Daude and P. Falgayrettes, "Near-field electromagnetic tomography applied to current density reconstruction in metallized capacitors," IEEE Transactions on Power Electronics, VOL. 20, no. 1, pp. 11-16, Jan. 2005.
- [13] C. Joubert, A. Bérroual, G. Rojat, "Magnetic Field and Current Distribution in Metallized Capacitors," Journal of Applied Physics, VOL. 76, No. 9, pp. 5288-52931 November 1994.
- [14] Jun Fan, "Near-field scanning for EM emission characterization," IEEE

Electromagnetic Compatibility Magazine, VOL. 4, no. 3, pp. 67-73, 3rd Quarter 2015.

[15] X. Gao, J. Fan, Y. Zhang, H. Kajbaf and D. Pommerenke, "Far-Field Prediction Using Only Magnetic Near-Field Scanning for EMI Test," IEEE Transactions on Electromagnetic Compatibility, VOL. 56, no. 6, pp. 1335-1343, Dec. 2014.

[16] Y. Liu, B. Ravelo, and A. K. Jastrzebski, "Calculation of time-domain near field  $E_{x,y,z}(t)$  from  $H_{x,y}(t)$  with PWS and FFT Transforms," in Proc. Int. Symp. Electromagn. Compat., Roma, Italy, pp. 1-6, 17-20 September 2012.

[17] B. Ravelo, "E-field extraction from H-near-field in time-domain by using PWS method," Progress Electromagn. Res. B, VOL. 25, pp. 171-189, 2010.

[18] Y. Liu, B. Ravelo, A. K. Jastrzebski, and J. B. Hadj Slama, "Calculation of the time domain z-component of the EM-near-field from the x- and y-components," in Proc. 41st Eur. Microw. Conf., pp. 317-320, 10 - 13 October 2011.

[19] G. J. Burke and A. J. Poggio, "Numerical Electromagnetics Code (NEC) - Method of Moments," NOSC TD 116 Part I, January 1981.

[20] J. Ben Hadj Slama, S. Saidi, "Coupling the Electromagnetic Inverse Problem Based on Genetic Algorithms with Moment's Method for EMC of Circuits," 15th IEEE Mediterranean Electrotechnical Conference MELECON'10, Malta, pp. 709-714, 26-28 April 2010.

[21] Sofiene Saidi and Jaleddine Ben Hadj Slama, "Effect of Genetic Algorithm parameters on Convergence of the Electromagnetic Inverse Method," 8th International Multi-Conference on Systems, Signals & Devices, pp. 1-5, 22-25 March 2011.

[22] Zitouna, B., Ben Hadj Slama, J., "Enhancement of time-domain electromagnetic inverse method for modeling circuits radiations," IEEE Trans. Electromagn. Compat., VOL. 58, (2), pp. 534-542, 2016.

[23] Bessem Zitouna and J. Ben Hadj Slama, "Time domain inverse method based on the near field technique to solve electromagnetic interference problems: application to an AC/DC flyback converter," IET Power Electronics, VOL. 11, no. 13, pp. 2133-2139, Jun. 2018.